Effective Sphere Modeling for Electrostatic Forces on Three-Dimensional Spacecraft Shapes

Lee E. Z. Jasper and Hanspeter Schaub

EFFECTIVE SPHERE MODELING FOR ELECTROSTATIC FORCES ON THREE-DIMENSIONAL SPACECRAFT SHAPES

Lee E. Z. Jasper[*] and Hanspeter Schaub[†]

Satellite formations utilizing Coulomb forces are being studied due to their potential for their extremely low-fuel, low-power close formation flying control. Prior studies into Coulomb formations employ point charge or isolated sphere assumptions with well known electrostatic behavior. This is justified by having the custom Coulomb spacecraft assume near-spherical shapes to minimize charge densities for a given potential. Complex geometries, however, are the norm for existing satellite structures. This paper develops a method to model complex geometries as finite spheres. Finite element electrostatic field solutions are used to model the force interactions between a sphere and a non-spherical body. The effective sphere method is demonstrated on a sphere, a cylinder and a generic satellite structure. Force behavior is shown to match between the finite element solution and a 3D body's effective sphere for separation distances beyond $3-4$ craft radii. Differences in the effective radii for the same non-spherical body are discussed along principal body axes and a near-elliptical distribution of effective radii are found for the case of a cylindrical shape. Finally, the nadir-aligned relative motion control of a cylinder-sphere formation is considered using the cylinder's effective radius and a voltage control strategy.

INTRODUCTION

Formation flying of spacecraft, through use of electrostatic (Coulomb) forces, have been the focus of research for many years.[1–4] Use of electrostatic forces to maintain a formation is appealing because the formation can be maintained with minimal use of fuel (I_{sp} values for relative motion control can reach up to $10^{13}s$) and low power consumption, often less than 1 Watt.[1,5] Thus, electrostatic forces allow formations to exist without the use of precious fuel and they avoid thruster exhaust plume impingement issues between spacecraft. Due to the cold and dense near-Earth plasma environment, the Debye lengths are only large enough to effectively use the Coulomb forces at high Earth and geosynchronous orbit (GEO) altitudes. However, at these high orbits, nominal minimal Debye lengths range from 180-200 meters, allowing for Coulomb spacecraft formations to be tens of meters in size.[6]

A common Coulomb formation studied is the simple two point-charge formation. This is used to study rendez-vous and docking applications,[7] virtual tethering of sensor probes to a mother craft,[8] electrostatic collision avoidance,[9] as well as creating virtual Coulomb structures.[10,11] The dynamics for two charged craft are much simpler than the complex N charged body problem. Even with the two-body problem the charge feedback control and stability development are challenging due

---

[*]Graduate Research Assistant, Aerospace Engineering Sciences Department, University of Colorado, Boulder, CO 80309-0431.

[†]Associate Professor, H. Joseph Smead Fellow, Aerospace Engineering Sciences Department, University of Colorado, Boulder, CO 80309-0431.

to the nonlinear electrostatic force actuations, and the coupling with differential gravity. This paper extends the discussion on two charged spacecraft. However, the focus is placed on finite bodies with three-dimensional shapes instead of only considering point charge models. Electrostatic properties of spherical bodies have been studied analytically for some time. Soules creates empirical models of the electrostatic forces between two finite spheres, including induced charging effects, using a modified method of images.[12] Experimental verification of such charge to voltage models of spheres is recently discussed in Reference 13. Neighboring finite bodies held at non-zero electrostatic potentials can create increased or decreased capacitance compared to the capacitance models of isolated bodies. The relation between the body size and separation distance leads to a position dependent capacitance matrix.[14,15] With these enhanced absolute voltage to charge relationships, the charge feedback control work in prior research efforts such as References 16, 17 and 18 can be reformulated as voltage control problems.

However, most currently flying spacecraft are not spherical in shape. For the electrostatic relative orbital dynamics research, it is of interest how well the three-dimensional electrostatic fields of generally shaped bodies can be modeled without having to resort to the time-intensive and complex finite element electrostatic field solutions. This paper first investigates how to represent the electrostatic force behavior between a sphere and a general shape by representing the three-dimensional shape with an equivalent finite sphere. This allows for complex geometries, with electrostatic behavior that cannot be solved in closed form, to be approximated with spherical models with known characteristics. Two effective spheres methods are considered and compared which differ in the complexity required to evaluate the effective sphere radius. The sphere representation allows for very fast evaluations of the electrostatic forces thanks to the analytical closed form solution. The scope of this study only considers line-of-sight electrostatic force solutions between the two the center of masses. Non-aligned forces and torques are not considered in this work. Further, of interest is over what separation distance range such simplified models yield reasonable electrostatic force approximations. If a spacecraft has long solar panels extended and deployed, then small separation distances can create strong induced charge distributions between the sphere and the nearby solar panel components.
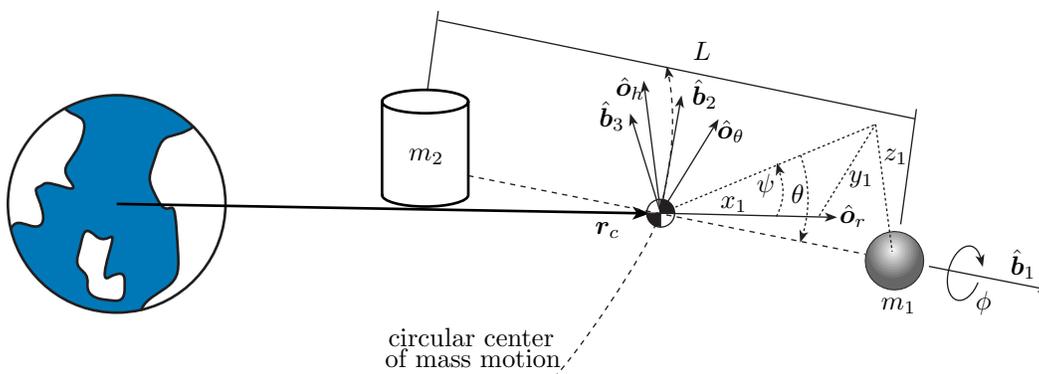
Figure 1. Illustration of a nadir-aligned charged two-craft formation.

Finally, the effects of considering finite bodies and the effective radius are demonstrated by revising the nadir-aligned charge feedback control study by Natarajan and Schaub.[8] This study uses a cylindrical body shape for one of the charged objects. Further, the prior Coulomb formation feed-

back control strategies utilize charge as the fundamental control variable.[19–23] This paper explores voltage control, instead of charge control, for a nominally nadir-aligned charged two-body system. Controlling the voltage is a more practical control variable as any charge emission device fundamentally controls the potential of a spacecraft, not directly charge. Reference 8 demonstrates that if both spheres are aligned in an orbit radial formation as illustrated in Figure 1, the overall formation is feedback stabilizable using only separation distance measurements. This paper investigates a modified feedback control strategy using voltages as the fundamental variable with the enhanced electrostatic force modeling.

SPHERE-SPHERE ELECTROSTATIC FORCE MODEL MODEL

Modeling of point charges uses the simple relation between voltage and charge:

$$V(q) = k_c \frac{q}{L} \tag{1}$$

where L is the separation distance, q is the point charge, and $k_c = 8.99 \cdot 10^9$ Nm^2/C^2 is the Coulomb constant. The force F between two charges q_1 and q_2 is:

$$F = -\nabla V(q_1) \cdot q_2 = k_c \frac{q_1 q_2}{L^2} \tag{2}$$

However, these equations only model point charge forces and not the inter-body electrostatic forces between general three-dimensional bodies. Specifically, when considering the case of finite bodies, any body's potential is dependent upon its own charge, as well as that of its neighbors. References 14 and 15 show that this alters Eq. (1) and changes it to:

$$V_i = k_c \frac{q_i}{r_i} + \sum_{j=1, j \neq i}^{n} k_c \frac{q_j}{L_j} \tag{3}$$

where n is the number of charged bodies. This is a linear equation and can be generalized to the matrix form:

$$\bar{V} = k_c [C_M]^{-1} \bar{q} \tag{4}$$

where $[C_M]^{-1}$ is the inverse of the position dependent capacitance matrix for the system, and assumes the following algebraic form:

$$[C_M]^{-1} = \begin{bmatrix} 1/R_1 & 1/L_{1,2} & ... & 1/L_{1,n} \\ 1/L_{2,1} & 1/R_2 & ... & : \\ : & ... & \ddots & : \\ 1/L_{n,1} & ... & ... & 1/R_n \end{bmatrix} \tag{5}$$

where R_i are the spherical radii of the bodies and $L_{i,j}$ are the distances between each body. If only two craft are flying in formation, as is the main assumption in this paper, then Eq. (4) becomes:

$$\begin{bmatrix} V_1 \\ V_2 \end{bmatrix} = k_c \begin{bmatrix} 1/R_1 & 1/L_{1,2} \\ 1/L_{2,1} & 1/R_2 \end{bmatrix} \begin{bmatrix} q_1 \\ q_2 \end{bmatrix} \tag{6}$$

The notation is simplified slightly because $L_{1,2} = L_{2,1}$, which is represented from now on as $L = L_{1,2}$. Given Eq. (6), as well as the size and distance between two finite bodies, the voltages

V_i can be computed given the total charges q_i on each sphere. Or conversely, each sphere's charge can be determined if a voltage is known. This second case, having a predetermined voltage, is of particular interest because it is much easier to create a specific potential on an object than a charge. This paper assumes that the absolute voltages on both bodies are known and that the voltages are taken relative to an absolute (0V) reference at infinity. Eq. (4) therefore allows the absolute charges q_i on multiple three dimensional finite spheres to be computed based upon given potential V_i. These charges are now used to solve for the force between two bodies (Eq. (2)).
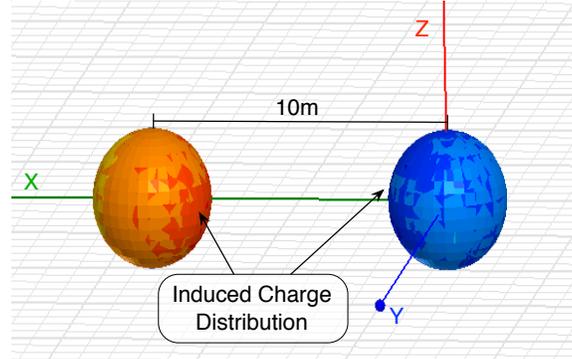
Figure 2. Sphere-sphere charge modeling.

To demonstrate the effectiveness of these analytic results, they are compared to the finite element program Maxwell3D, which solves the full Poisson's equations. As shown in Figure 2, two spheres of equal radius (2 meters) are placed at varying distances L apart. The sphere at the origin is given a fixed potential of 25kV, while the variable-distance sphere is given a -25kV fixed potential. Maxwell3D computes the center-to-center forces for each separation distance considered. The results are next compared to the analytic solution using Eq. (6) and Eq. (2).

Figure 3 demonstrates how the point charge model for the force in Eq. (2) relates to the combined capacitance model that solves for charges using Eq. (6). Once the coupled effects are taken into account, the force noticeably increases for smaller separation distances. The induced effects add onto the coupled charge force model at close distances (within about 2 - 3 craft radii). One point of interest is that the force in between the spheres is higher than originally expected with the point charge model. Therefore, when coupled capacitance is accounted for, higher forces (and possibly more control authority) occurs for a given absolute voltage.

Using the sphere-sphere model, Figure 3 shows both induced and coupled capacitance force effects of 3D shapes. Induced force effects are caused by the fact that some parts of the 3D shapes are closer than others. This makes charge concentrate on the surfaces nearest each other (Figure 2). The charge movement makes the effective separation distance smaller than the center-to-center distance used in the classical point charge equation, thus providing an increased force in relation to that of Eq. (2). The analytical sphere-sphere force model presented here uses a method developed by Soules in Reference 12 to estimate the induced effects between two spheres. When the induced behavior is taken into account, the coupled capacitance model very closely models the high-fidelity numerical results. Figure 3 demonstrates that at distances less than 3 - 4 craft radii, the coupled capacitance and induced force models are necessary to model sphere-sphere interaction. Beyond that distance, the coupled capacitance model provides a very good fit to the numerical results.
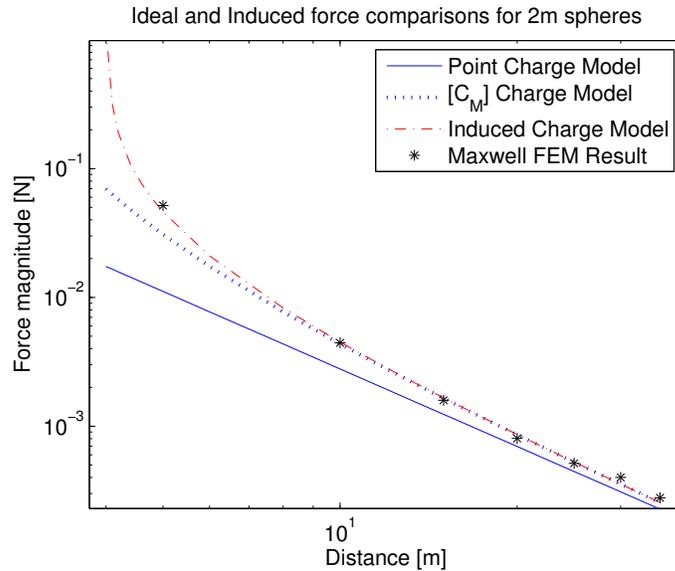
Figure 3. **Ideal and Induced force comparisons for 2 m spheres.**

1$^{\text{ST}}$ ORDER EFFECTIVE RADIUS METHOD

Algorithm Description

While the sphere-sphere electrostatic interaction is useful for demonstration purposes, it does not closely relate to the geometry of actually deployed spacecraft. Therefore, it is of interest to study generic 3D shapes and their electrostatic interaction with a spherical vehicle. It is beyond the scope of this paper to consider interactions between multiple 3D shapes. However, while non-spherical shapes are more realistic, there are no analytic solutions for describing how spherical objects will interact with another charged object. While analytical solutions for non-spherical shapes might be possible to find, they are extremely difficult to develop. Finite element codes can also be used, however, these can be computationally intensive and they do not provide a generalized perspective on the system's electrostatic force behavior.

In an effort to make complex three dimensional shapes easier to analyze, a method is developed to find a body's effective spherical radius. A complex shape is approximately modeled as a a finite sphere by fitting its electrostatic Coulomb force characteristics to the spherical model of Eq. (4). Considering, again, the charged two-body system, Eq. (6) is used.

Figure 4 demonstrates the problem set-up for this method called the 1$^{\text{st}}$-Order Effective Sphere Method. A sphere and a cylinder are placed within a small number of craft dimensions of each other. The voltages on both bodies are known and held fixed, and the spherical body's radius R_1 is known. The center-to-center force F between the two objects is computed using a finite element numerical solver, such as Maxwell3D. Knowledge of all of these parameters, including the separation distance between the two bodies, allows for the cylinder's effective sphere to be calculated using the following procedure. To calculate the effective radius R_2 of the cylinder, the three unknown parameters of the system (q_1, q_2, R_2) must be solved for simulateneously. To find
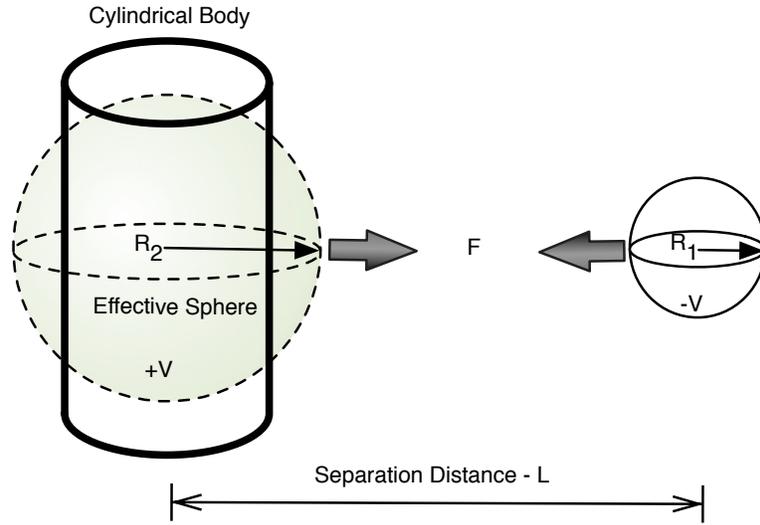
Figure 4. Example of a cylinder modeled as an effective sphere.

expressions for q_1 and q_2, Eq. (6) is separated into two equations.

$$V_1 = k_c \left(\frac{q_1}{R_1} + \frac{q_2}{L} \right) \tag{7}$$

$$V_2 = k_c \left(\frac{q_1}{L} + \frac{q_2}{R_2} \right) \tag{8}$$

Because the force F is known from the finite element solution at a particular configuration, q_2 is solved from Eq. (2) as a function of q_1:

$$q_2 = \frac{FL^2}{k_c q_1} \tag{9}$$

There are now three equations with three unknowns: q_1, q_2, R_2. Substituting Eq. (9) into Eq. (7) yields the following quadratic function of q_1:

$$0 = \frac{q_1^2}{R_1} - \frac{V_1}{k_c} q_1 + \frac{FL}{k_c} \tag{10}$$

This quadratic equation is solved for q_1. Because q_1 is now known, q_2 is solved for using Eq. (7). All parameters are now known in Eq. (8) except for the effective radius, R_2. R_2 can be easily solved for to obtain the second body's effective spherical radius:

$$R_2 = q_2 \left(\frac{V_2}{k_c} - \frac{q_1}{L} \right)^{-1} \tag{11}$$

Note that the computed effective radius is only accurate for the given geometry used in the finite element numerical solution. If the cylinder in Figure 4 is rotated relative to the sphere, different forces will be experienced, resulting in a different effective radius. Thus, this method of evaluating

6

a 1$^{\text{st}}$-order effective radius must be repeated if another relative orientation of general shape and sphere are considered. This relative orientation dependent effective radius behavior is investigated further in the following sections.

To gain some insight into the behavior of Eq. (10), q_1 is solved for using the quadratic equation:

$$q_1 = \frac{V_1 R_1}{2k_c} \pm R_1 \sqrt{\frac{1}{4}\frac{V_1}{k_c}^2 - 4\frac{FL}{R_1 k_c}} \tag{12}$$

As a simple check of this method, assume the force F is zero. Using the positive root, then the expression for q_1 simplifies to the expected single sphere voltage and charge relationship:

$$q_1 = \frac{V_1 R_1}{k_c} \tag{13}$$

For an attractive case, $F < 0$, which increases the size of q_1. For a repulsive case , $F > 0$, which decreases the size of q_1, as expected.

Because the expression for q_1 is a quadratic expression, there are two possible solutions. To understand whether the positive or negative solution for q_1 should be used, R_2 is solved for another way. R_2 can be solved for by taking Eq. (6), solving for both charges, and then plugging them into Eq. (2), which provides a quadratic equation for R_2. If this is done and the equations are solved using the physical constraints for an attractive system (i.e. $R_1 > 0$, $L > 0$, V_1 = -V_2 thus $F < 0$) a simplified equation for R_2 is found. This expression produces two roots, one negative and one positive. This guarantees that there will always be one physically possible solution for this method ($R_2 > 0$) and that there are no non-unique solutions.

When the effective radius is computed, a unique radius is computed for each force and separation distance tested. By evaluating the effective radius $R_{2,i}$ for a set of N separations L_i, the final 1$^{\text{st}}$-order effective radius R_2 is evaluated as the mean of all evaluated radii.

$$R_2 = \frac{1}{N}\sum_{i=1}^{N} R_{2,i} \tag{14}$$

Next, appropriate ranges of separation distance for the numerical electrostatic force evaluation are considered. Due to induced charge effects and resulting larger electrostatic forces between three-dimensional bodies, short separation distances can produce effective radii that are larger than the general force trend that occurs at larger distances. Because the above effective radius evaluation for a given set of potentials and separation distance does not include the induced charge effect, the numerical finite element electrostatic force evaluations should consider separation distance larger than 3-4 craft radii. This yields an good effective sphere fit for the general shape. Further, the induced effects can be added to the effective sphere to increase the force modeling accuracy for small separation distances.

Sphere-Sphere Algorithm Verification

To demonstrate the accuracy of the 1$^{\text{st}}$-order effective radius method, a sphere-sphere system (Figure 2) is considered with each sphere's radius being 2 meters. The effective radius of sphere 2 is then calculated assuming its, radius R_2, is unknown. Both spheres are given fixed equal magnitude and opposite sign potentials of $\pm$ 25kV.
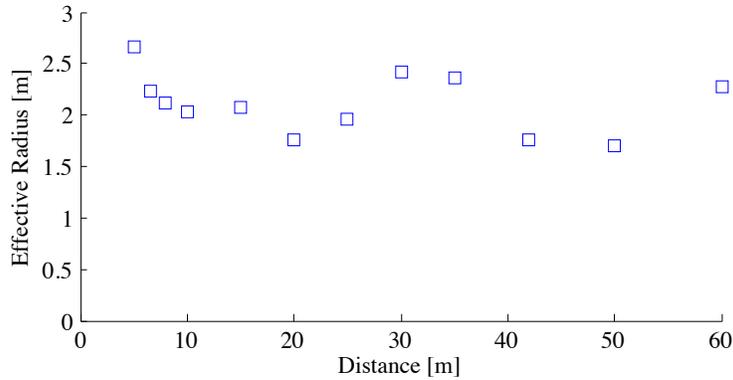
Figure 5. Effective radii calculated at different distances between two 2m spheres.

The effective radii $R_{2,i}$, calculated using Eq. (11) for each separation distance L_i, are shown in Figure 5. Induced effects on the effective radius are seen before 10m. Beyond 20m the effective radii calculations are increasingly noisy. This is caused by Maxwell3D attempting to evaluate vanishingly small electrostatic forces, resulting in relatively noisy force evaluations. Assuming this noise is random and Gaussian, its average value should equal the true effective radius. However, consider that the induced effects are not random. The effective radii computed where the induced effects are significant should be ignored. The effective radii for separation distances beyond 10m are run through a least squares fit algorithm for a zero slope line. This produces an effective radius of 2.04m, which is very close to the actual 2m sphere modeled in Maxwell3D. If all effective radii are considered including separation distances where the induced charge distribution is significant, then an increased average radius of 2.11m is computed, as expected. This shows that ignoring the effective radius data at the distances where induced force effects are significant produces more accurate effective radii, and therefore force results. In Figure 6 the relative force error is compared between the true 2m-2m sphere system, Maxwell3D's FEM results, and the two calculated effective radii. The 2.04m estimate yields only about 2 percent error while the 2.11m radii produces about 6 percent error. Again, this demonstrates that Maxwell3D produces slightly noisy force data at separation distances beyond 20m but that the average of the effective radii produced by this data gives reasonably good estimates for the behavior of the 3D shape.

Relative Orientation Dependence

Computing the effective radius of a known sphere has helped illustrate the numerical accuracy of this method, as well as justification for ignoring induced effective radii results. This knowledge is next applied to a cylinder with an unknown effective electrostatic radius. With the simple sphere-sphere scenario, the relative orientation of the two objects did not matter. With general shapes this is not true, as discussed earlier.

Considering a more complex shape, a cylinder 3 meters in radius and 12 meters in height is modeled as object 2. The sphere 1 has a radius of two meters and the vehicles are charged to $\pm$ 25kV. If the sphere moves or the cylinder rotates, the force behavior between the two bodies changes and a different effective radius R_2 must be computed. If the sphere changes position and is no longer as shown in Figure 4, but instead at an off-axis position relative to the cylinder, the

8
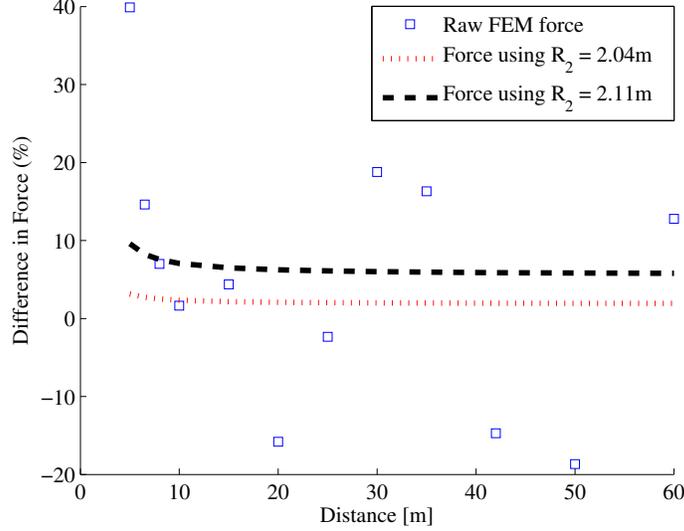
Figure 6. Relative force error between true (R_2 = 2m) and other force estimates.

charges and forces change between the two objects, graphically shown in Figure 7. As the sphere rotates about the cylinder, the effective radii is postulated to change in an elliptical pattern. To numerically illustrate this pattern, the reference sphere is placed around the cylinder at multiple points between the $\hat{c}_1$ axis to the $\hat{c}_3$ axis. Multiple separation distances between the center of the sphere and cylinder are used to calculate the effective radius for a given angle ϕ_2. An individual effective radius is calculated for each angle about the cylinder by the averaging process described above.

Figure 8 illustrates the resulting effective radii for a range of relative orientations. For the sphere-cylinder case considered, the effective radius varies as an ellipse where the major ellipse axis is the length of the long, $R_{2,3}$ axis effective radius, and the minor ellipse axis is the length of the $R_{2,1}$ effective radius. Because the numerically evaluated effective radii of a cylinder-sphere scenario appear to vary in a predictable manner, only the effective radii of a cylinder's radial and axial axes need to be determined to be able to model the electrostatic force behavior of the cylinder in the neighborhood of sphere. Due to the symmetry of the cylinder, the elliptical behavior can be expanded to an ellipsoid shape with the minor and intermediate principal axes of the ellipsoid being the same length ($R_{2,1}$). If the ellipsoid is parameterized into a local 'ellipsoid' frame shown in Figure 7, any point on the effective radius ellipsoid surface is expressed by the equations:

$$x = R_{2,1} \cos \phi_2 \cos \phi_1 \tag{15a}$$

$$y = R_{2,2} \cos \phi_2 \sin \phi_1 \tag{15b}$$

$$z = R_{2,3} \sin \phi_2 \tag{15c}$$

where the effective radius acting between the sphere and cylinder is:

$$R_2 = R_{\text{eff}} = \sqrt{x^2 + y^2 + z^2} \tag{16}$$

If the cylinder is rotating or tumbling both the orbit frame angles (θ, ψ from Figure 1) and the attitude of the cylinder need to be accounted for in Eq. (15a). Linearizing Eq. (16) for small angles

9
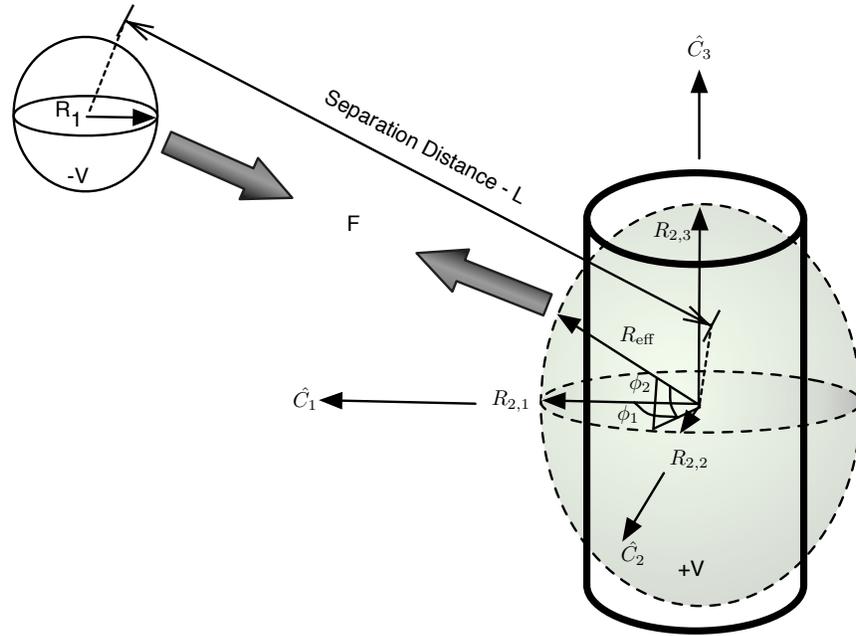
Figure 7. Ellipsoidal effective radius behavior as a sphere rotates about a cylinder.

about the principle axes of the ellipsoid, the effective radius simply becomes the radius of the given axis, i.e. $R_2 = R_{2,1} = R_{\text{eff}}$ if linearized about $\phi_1 = \phi_2 = 0$. This fact makes formation dynamics simpler if constant attitudes are held between the cylinder and sphere. Elliptical distributions of the effective radius may not occur for every 3D body geometry and should be verified for each unique geometry.

Effective Radius Robustness to Voltage Variations

The above discussion consideres many of the variables that affect the value of the effective radius. For example, separation distance, for long enough distances, provides constant effective radii. The physical orientation between two bodies changes the effective radius. However, for a cylinder-sphere scenario the radius changes in a predictable, ellipsoidal trend. Finally, the effects of changes in voltage are considered. Eq. (10) depends upon the voltage between the two craft but, it is uncertain whether changes in voltage will cause the effective radius to change. Thus, a sweep across voltages is performed holding the cylinder and sphere in the orientation seen in Figure 4. Figure 9 is obtained by changing the voltage on both bodies (equal and opposite) and then calculating the effective radius. Figure 9 numerically demonstrates that, over the ranges of voltages considered, the effective radius changes very little. The worst deviation is at 10kV and 3.8kV where the effective radius is 4.52m instead of 4.54m. Thus, the 1st-order effective sphere concept can provide realistic line-of-sight electrostatic force predictions for general shapes without having to evaluate effective radii for different voltage ranges. This makes this concept very practical to use this simplified electrostatic force instead of finite elements to compute faster than real-time control simulations.
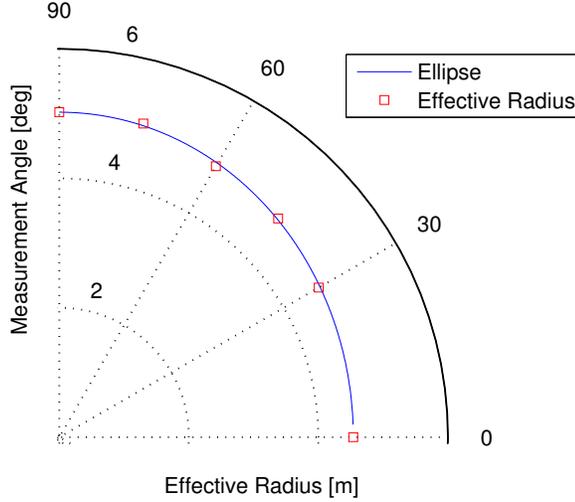
Figure 8. **Polar plot for elliptical effective radius made from R_{2x} = 4.54 m and R_{2z} = 5.02 m.**

0$^{\text{TH}}$ ORDER EFFECTIVE RADIUS METHOD

If the earlier effective radius method is considered a first-order approximation to the true electrostatic behavior of a multi-body system, then this next section discusses a simplified and less accurate 0$^{\text{th}}$ order approximation. The 1$^{\text{st}}$-order method requires extensive and time consuming finite element solutions to be evaluated to generate the effective radius. For a cruder, but much faster, approximation of the effective radius, the outer spacecraft surface area A is simply mapped onto a spherical shape.

$$R_{2_0} = \sqrt{\frac{A}{4\pi}} \tag{17}$$

The main benefits of this method is the speed at which an effective radius can be evaluated for a general shape. However, note that this 0$^{\text{th}}$-order method cannot account for relative orientation differences. Of interest is how much accuracy is sacrificed for the faster setup. Table 1 shows three different cylinder sizes that were modeled in Maxwell3D and then used with the effective radius method. This table compares electrostatic force modeling accuracy of the 1$^{\text{st}}$-order method to that of the 0$^{\text{th}}$-order method. Most of the force modeling difference are only a few percentage for the three cylinders considered. The largest difference is found along the cylinder symmetry axis and can reach up to 11%. This simplified model is adequate for many approximate electrostatic force evaluation where precision relative motion predictions are not required.

NUMERICAL EFFECTIVE SPHERE ACCURACY STUDY

Cylindrical-Sphere Model

To demonstrate the results from the use of the effective radius method in Eq. (11), a cylinder and spherical system is considered. A cylinder is used because it is a common space object shape. It
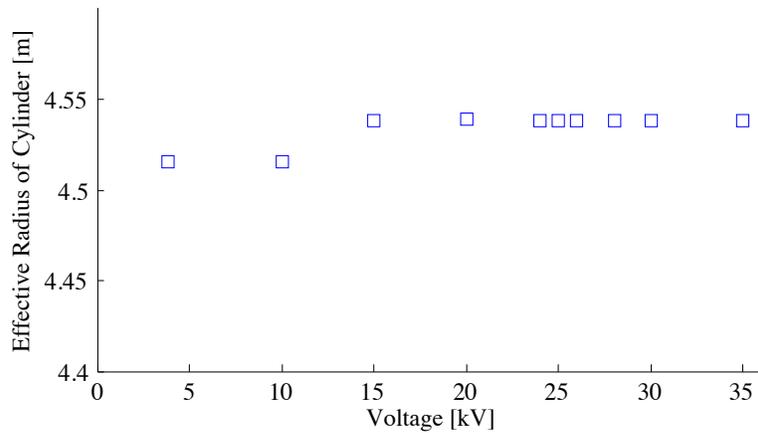
Figure 9. Effective radius for varying voltages for a cylinder and sphere along the X axis.

Table 1. Surface Area's of several cylinders and their zeroth order effective radius approximation.

Object	R [m]	H [m]	0th order R [m]	1st order R 'x' and 'y' [m]	1st order R 'z' [m]	Percent diff X, Y	Percent diff Z
Dual Spin S/C	1.85	6.8	2.83	2.78	2.62	1.77	7.42
Delta IV rocket body	2	10	3.46	3.57	3.82	3.18	10.40
Large rocket body	3	12	4.74	4.54	5.02	4.22	5.91

could be representative of a rocket body or dual-spin spacecraft, both of which can be found often near the GEO belt. Similar to the previous analysis the cylinder's dimensions are 3 meters in radius and 12 meters in height. The sphere has a radius of two meters. The cylinder has a voltage of positive 25kV and the sphere has a -25kV potential. Using Maxwell3D to find the center-to-center forces between the cylinder and sphere, the effective radius of the sphere is solved for using Eq. (9) through Eq. (11).
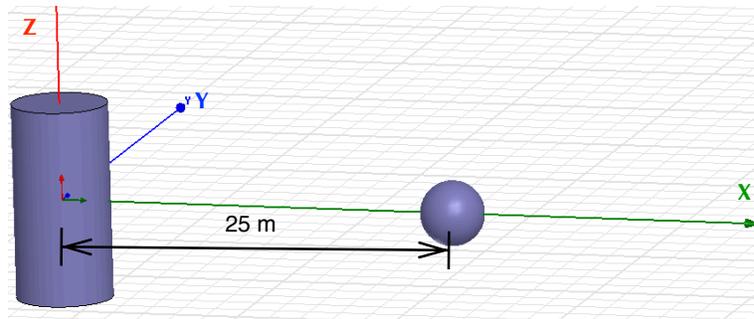
Figure 10. Sphere and cylinder geometry set-up.

Figure 11 shows the Maxwell3D results (points), and the force calculated using the effective radii method (lines). Forces created in both the X and Z axes are shown. Because the cylinder has two unique geometries as seen by the sphere, the effective radii calculated are different, but vary by

12
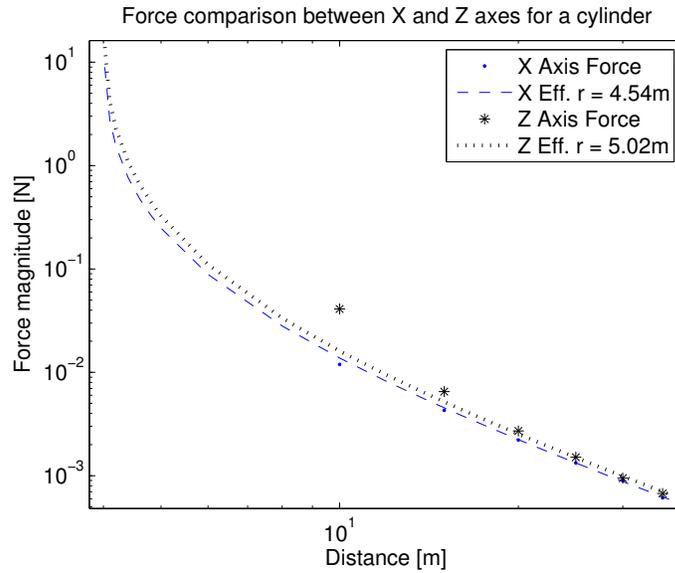
Figure 11. Force comparison between X and Z axes for a cylinder.

only about 9.5 percent. The effective sphere model does match the numerical results very well for separation distances of about 15 - 20 meters and beyond, for both axes. This demonstrates that the effective sphere method can indeed predict the behavior of a non-spherical body when separation distances are on the order of 3 - 4 craft radii away. Note that the forces in Figure 11 are plotted in a log-log scale. This was done to emphasize that the force behavior becomes nearly linear at distances beyond induced effects. This linear trend should therefore contain the dominant information about the system, including the effective radius of the cylinder. Indeed the logarithm of Eq. (2) becomes:

$$\log(F) = \log(k_c) + \log(q_1) + \log(q_2) - 2\log(L) \tag{18}$$

The effective radius method does not predict the force behavior accurately at ranges closer than $3 - 4$ craft radii, where induced effects begin to dominate. Figure 11 demonstrates the model's ability to fit an effective radius to the cylinder for two distinct orientations. The effective radii shown in Figure 11 are simply the two extrema for the body and the effective radii vary as an ellipse as shown in Figure 9. While the model for the induced effects between two spheres has been included in the force computation, this model becomes less accurate for a non-spherical body primarily because the geometry of the cylinder at close separation distances, becomes much more important. Further, it can be seen in Figure 11 that the Z axis behavior begins to vary from the effective radius model much more significantly than the X axis. This is partially caused by the fact that the current effective radius model only accounts for center-to-center separation distances. However, at center-to-center separation of 10 meters, the cylinder and sphere are actually only physically separated by 2 meters due to the cylinder having a height of 6 meters above its center, and the sphere having a radius of 2 meters. Thus the two objects are physically much closer than the effective radius model computes. Future work with effective radii might attempt to account for these differences between the physical system and the approximated system. Still, beyond 3–4 craft radii, the effective radius model matches the numerical results closely.

Table 2. Generic satellite body dimensions.

Component	X (or radius) [m]	Y (or height) [m]	Z [m]
Body	1.8	1.7	1.75
Dishes (x2)	.85	.3	0
Solar Panels (x2)	1.75	5.4	n/a

Generic Satellite - Sphere Model

Another, more complex shape is briefly considered. Figure 12 shows a generic satellite bus with a 2 meter sphere. The satellite's dimensions are roughly 14.3 meters from solar panel tip to tip, 6 meters in height between the dishes, and 1.7 meters in width.
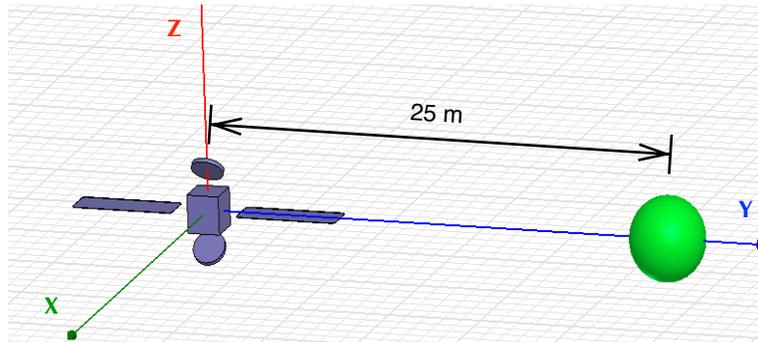
Figure 12. Generic satellite bus with a sphere.

This model represents a significantly more complex shape. Table 2 shows the dimensions used for the satellite body, not including separations between the body, dishes, and panels. Figure 13 demonstrates forces computed by the finite element and the effective radius methods. At close distances, the effective radius method poorly matches FEM results however, the models both closely match at and beyond 15 meters, just like the cylinder-sphere example in Figure 11. This demonstrates the versatility and effectiveness of the effective radius method. Even with complex geometry, the effective radius method models the force behavior between the satellite and the sphere allowing for easier force modeling behavior between complex geometries.

For a cylinder the effective radii between X and Z axes (Figure 11) vary by only about 9.5 percent. Likewise, the difference in the effective radii between the satellite's three axes (Figure 13) is only 22 percent between the Y and Z axes, and 2 percent between the X and Y axes. This shows that while geometry does change the effective radius of a body, its effects are not large as might be suspected.

Table 3 shows a 1st order versus 0th order radius calculations for the generic satellite. Along the X and Z axes, the 1st order and the 0th order methods match closely. However the Y axis, or the solar panel axis, produces noticeably different effective radii. This demonstrates that while the 0th order method can be used for rough approximation of the force behavior, for more extreme geometry, such as long extended panels, the method is not nearly as accurate as the 1st order effective radius method presented above.

14
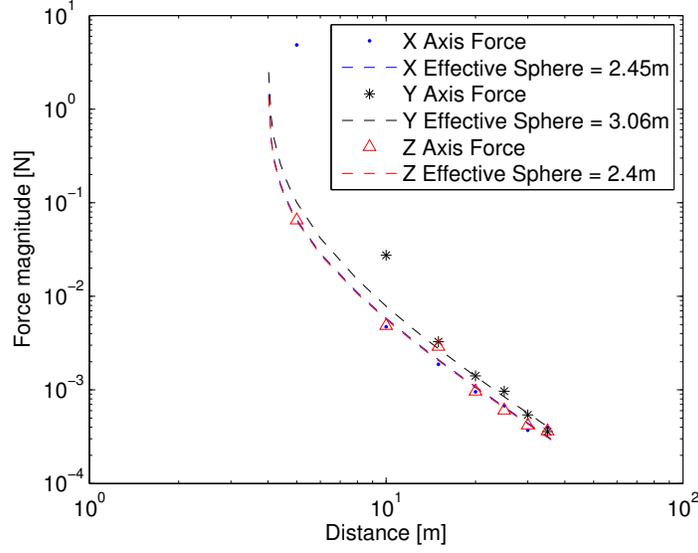
Figure 13. Force between satellite and sphere, in all three axes.

Table 3. Surface area's of a generic satellite shape and its 0th order effective radii for all three axes.

Object	0th order R [m]	1st order R 'x' [m]	1st order R 'z' [m]	1st order R 'y' [m]	Percent diff X	Percent diff Z	Percent diff Y
Generic S/C	2.33	2.40	2.45	3.06	2.91	4.90	23.86

VOLTAGE CONTROL OF A CYLINDRICAL AND SPHERICAL SPACECRAFT IN OR-BIT

Most research thus far into Coulomb formation flying satellites has used a body's charge as the control parameter. However, in practice, craft potential will likely be the control parameter. Eq. (4) can be used to transfer charge control strategies to voltage control. If a two craft system is considered, Natarajan and Schaub have shown that two craft aligned in an orbit radial direction are in a stable configuration (Figure 1). They also demonstrated that the motion in the radial (L), and rotation about the in-track vector (ψ) were coupled and could be stabilized. Following the development in Reference 8, the Hill-frame dynamics are rotated into a spherical frame, which allow for some decoupling of the equations of motion. The linearized differential equation for the separation distance, in the spherical frame (L,ψ,θ) is given as:

$$\ddot{L} = \left(2\Omega\dot{\psi} + 3\Omega^2\right) L + (k_c/m_1) Q \left(1/L^2\right) \left[(m_1 + m_2)/m_2\right] \tag{19}$$

Here, $Q = q_1 q_2$ is the charge product of the two craft and Ω is the orbit mean motion. Eq. (19) developed by Reference 8 assumes two point charges in formation however this equation remains true for a cylinder and sphere system when the effective radius method is used. The fact that point charge developments can still be used by the effective sphere model, is one of the primary advantages of the effective sphere model. This is justified by the fact that the charge Q accounts for the finite size of the objects when the coupled capacitance is included in the calculation of the charge

15

product. Using Eq. (6), the position dependent capacitance matrix can be used to get solutions for each body's net charge as a function of voltage. These charges can then be multiplied together to make $Q = f(V)$. Substituting the new charge product into Eq. (19) and linearizing the equation for small changes in separation distances and voltages, Eq. (19) becomes:

$$\delta \ddot{L} = 2L_{\text{ref}}\Omega\dot{\psi} + \left(3\Omega^2 + k_1\right)\delta L + k_2\delta V \tag{20}$$

where

$$k_1 = \frac{2R_2R_1(m_1 + m_2)(R_2^2R_1 + L_{\text{ref}}^2(2L_{\text{ref}} + 3R_1) + R_2(3L_{\text{ref}}^2 + 6L_{\text{ref}}R_1 + R_1^2))V_{\text{ref}}^2}{k_cm_1m_2(L_{\text{ref}}^2 - R_2R_1)^2} \tag{21}$$

and

$$k_2 = -\frac{2R_2R_1(R_2 + L_{\text{ref}})(m_1 + m_2)(L_{\text{ref}} + R_1)V_{\text{ref}}}{k_cm_1m_2(L_{\text{ref}}^2 - R_2R_1)^2} \tag{22}$$

Note that V_{ref} is the nominal reference voltage for the system and L_{ref} is the reference separation distance, both values are constants. Reference 8 shows that the reference charge (for a stable orientation for a given L_{ref}) is:

$$Q_{\text{ref}} = q_1q_2 = -\frac{3\Omega^2 L_{\text{ref}}^3 m_1m_2}{k_c(m_1 + m_2)} \tag{23}$$

The reference voltage can then be computed using Eq. (6) assuming the charges are $\pm\sqrt{|Q_{\text{ref}}|}$, respectively. This means that both Eq. (21) and Eq. (22) are constant values if the relative motion between both bodies is small and aligned along a principal axis of the cylinder/ellipsoid of Figure 7. Note that R_2 is the effective radius found from the ellipsoidal distribution from Figure 7 and Eq. (16). If the cylinder were tumbling, the sphere were rotating around the cylinder, or an off principle-axis orientation were being held, R_2 would not be constant and k_1 and k_2 would not be constant, significantly increasing the complexity of Eq. (20).

Making a feedback control law similar to the control developed by Reference 8, the voltage is given as:

$$\delta V = 1/k_2\left(-C_1\delta L - C_2\delta\dot{L}\right) \tag{24}$$

This control yields the following linearized closed-loop separation distance dynamics:

$$\delta \ddot{L} = 2L_{\text{ref}}\Omega\dot{\psi} + \left(3\Omega^2 + k_1 - C_1\right)\delta L - C_2\delta\dot{L} \tag{25}$$

Here the positive C_1 and C_2 parameters are control gains and both proportional and derivative feedback are given to ensure asymptotic stability. The linearized equations of motion for the in-track and cross-track rotations are unchanged in Reference 8's development and are given for ease of reference:

$$\ddot{\psi} = -\left(2/L_{\text{ref}}\right)\delta L - 3\psi \tag{26}$$

$$\ddot{\theta} = -4\theta \tag{27}$$

(a) $\sqrt{\psi^2 + \theta^2}$ residuals
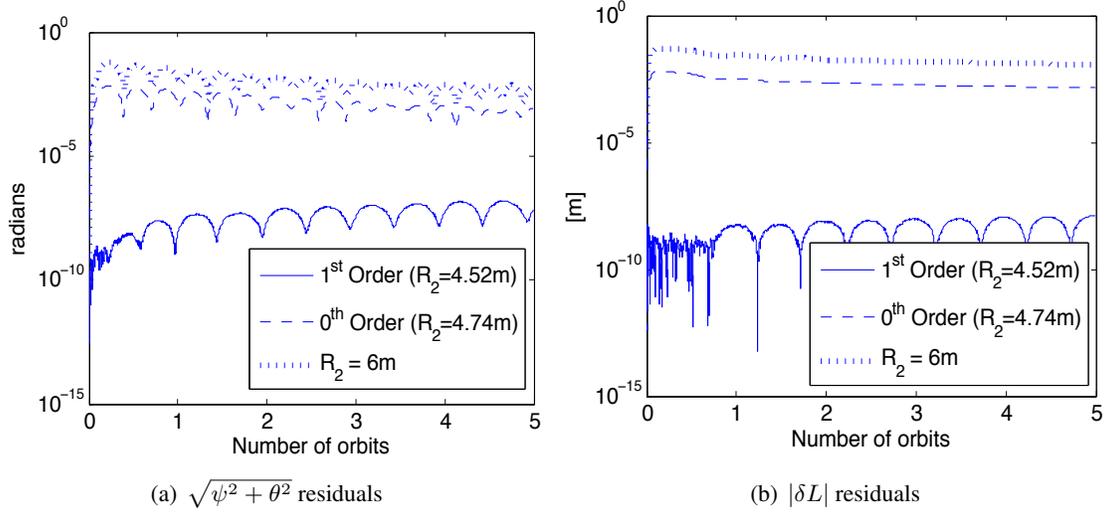
(b) $|\delta L|$ residuals

Figure 14. Residual motions relative to a true effective sphere of $R_2 = 4.524$m at 25m separation distance.

Choosing gains C_1 and C_2 as outlined in Reference 8 results in the values:

$$C_1 = 25\Omega^2$$
$$C_2 = 9.12\Omega$$

Integrating the full nonlinear inertial equations of motion that account for coupled position dependent capacitance and a voltage based control, the behavior of the two craft system can be obtained. Here $L_{\text{ref}} = 25$m, $V_{\text{ref}} = 3750$V, $R_1 = 2$m. A range of effective radii are considered, ranging from $R_2 = 4.74$m for the 0th order method as computed in Table 1, $R_2 = 4.52$m for the 1st order method as shown in Figure 9 and $R_2 = 6$m estimating the effective radius as half the height of the cylinder. The initial separation deviation and attitude are $\delta L = .5$m, $\psi = \theta = 0.1$ rad and $\delta \dot{L} = \dot{\psi} = \dot{\theta} = 0$. Note that setting V_{ref} to 3750V is the proper reference voltage for an effective radius of 4.52m and that the other estimates will not satisfy the necessary reference charge to settle to a zero δL offset. Figure 15 demonstrates the motion of the craft from a relative reference separation distance (L_{ref}) of 25 meters and that voltage control does indeed stabilize the same configuration as the charge based control. However, small errors can be seen for the 0th order method and larger errors on the order of 2.5m for δL can be seen for the $R_2 = 6$m effective radius (overestimate).

Note that the control stabilizes the separation distance and the in-track rotation, but not the cross-track rotation. When observing the linearized analysis in Eq. (26) and Eq. (27) this behavior is apparent considering that δL occurs in Eq. (26) but not in Eq. (27), rendering the θ response that of a simply a harmonic oscillator. The continuing oscillation of ψ and δL after about 3 orbits is due to differential gravity that the linearized control does not effectively counter.

Figure 15 demonstrates how well each effective radius produces the proper forces to achieve the true inertial dynamics at 25m separation. The 'truth' model was produced by calculating the effective radius for the cylinder-sphere system at 25m separation. This effective radius ($R_{2\,\text{true}} = 4.524$m) exactly matches the steady state force at $L_{\text{ref}} = 25$m and therefore it produces the true dynamic response at 25m. Figure 14 gives a better example of how close the dynamics behave

17
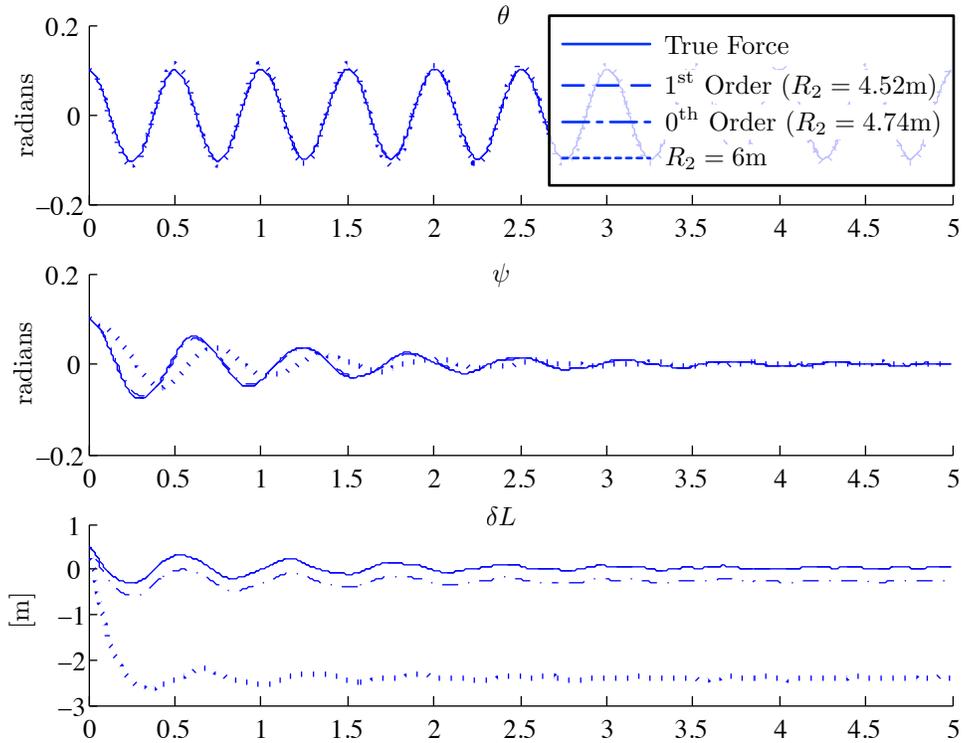
Figure 15. Voltage control craft response for different effective radii estimates.

using the approximated forces. Figure 14(a) shows the residuals for the formation orientation error measure $\sqrt{\psi^2 + \theta^2}$ and Figure 14(b) illustrates the $|\delta L|$ errors, compared to the truth simulation. This shows that basing the effective radius off of geometry dimensions alone produce largely varying force estimates. The 0th-order method produces reasonably accurate dynamics for high level analysis. Finally, the computation of the effective radii using the 1st-order method can produce force behavior that varies minimally compared to the full equations of motion demonstrating how powerful this method can be.

CONCLUSION

Prior research has modeled the Coulomb spacecraft as points or isolated spheres. This paper models complex geometries using finite spheres by calculating their effective radii through each body's force interaction with a sphere of known radius. This analysis, combined with a coupled position dependent capacitance matrix, allows for force behavior between a sphere and a 3D body to be modeled as two spheres. While the effective radius method requires *a priori* knowledge of the force behavior (in this case, through finite element modeling), the method accurately models the force interactions between two bodies making all successive calculations simpler. The electrostatic torques are not modeled with this approach. A simplified 0th-order effective sphere evaluation only uses the outer surface area to compute a radius, yielding difference ranging from 5-30% depending on the object shape and relative orientation. For a 3D body shaped like a cylinder, the effective radius changes over the body orientation in an elliptical manner. A voltage-based control illustrate the use of effective radii in enhanced control simulations.

REFERENCES

[1] J. H. Cover, W. Knauer, and H. A. Maurer, "Lightweight Reflecting Structures Utilizing Electrostatic Inflation," US Patent 3,546,706, October 1966.

[2] H. Schaub, G. G. Parker, and L. B. King, "Challenges and Prospect of Coulomb Formations," *Journal of the Astronautical Sciences*, Vol. 52, Jan.–June 2004, pp. 169–193.

[3] L. B. King, G. G. Parker, S. Deshmukh, and J.-H. Chong, "Study of Interspacecraft Coulomb Forces and Implications for Formation Flying," *AIAA Journal of Propulsion and Power*, Vol. 19, May–June 2003, pp. 497–505.

[4] L. Pettazzi, H. Krüger, S. Theil, and D. Izzo, "Electrostatic Forces for Satellite Swarm Navigation and Reconfiguration," *2nd ACT Workshop on Innovative Concepts*, ESTEC, 2008.

[5] L. B. King, G. G. Parker, S. Deshmukh, and J.-H. Chong, "Spacecraft Formation-Flying using Inter-Vehicle Coulomb Forces," tech. rep., NASA/NIAC, January 2002. http://www.niac.usra.edu.

[6] A. C. Tribble, *The Space Environment - Implications for Spacecraft Design.* Princton University Press, revised and expanded ed., 2003.

[7] A. Natarajan and H. Schaub, "Orbit-Nadir Aligned Coulomb Tether Reconfiguration Analysis," *Journal of the Astronautical Sciences*, Vol. 56, Oct. – Dec. 2008, pp. 573–592.

[8] A. Natarajan and H. Schaub, "Linear Dynamics and Stability Analysis of a Coulomb Tether Formation," *AIAA Journal of Guidance, Control, and Dynamics*, Vol. 29, July–Aug. 2006, pp. 831–839.

[9] S. Wang and H. Schaub, "Electrostatic Spacecraft Collision Avoidance Using Piece-Wise Constant Charges," *AIAA Journal of Guidance, Control, and Dynamics*, Vol. 33, Mar.–Apr. 2010, pp. 510–520, DOI:10.2514/1.44397.

[10] J. Berryman and H. Schaub, "Analytical Charge Analysis for 2- and 3-Craft Coulomb Formations," *AIAA Journal of Guidance, Control, and Dynamics*, Vol. 30, Nov.–Dec. 2007, pp. 1701–1710.

[11] S. Wang and H. Schaub, "Nonlinear Coulomb Feedback Control of a Spinning Two Spacecraft Virtual Structure," *Advances in Astronautical Sciences*, Vol. 135, American Astronautical Society, 2009, pp. 1477–1496. Paper AAS 09–393.

[12] J. A. Soules, "Precise Calculation of the Electrostatic Force Between Charged Spheres Including Induction Effects," *American Journal of Physics*, Vol. 58, 1990, pp. 1195–1199.

[13] C. R. Seubert and H. Schaub, "Electrostatic Force Model for Terrestrial Experiments on the Coulomb Testbed," *61st International Astronautical Congress*, Prague, CZ, International Astronautical Federation, Sept. 2010. Paper IAC-10.C1.1.9.

[14] W. R. Smythe, *Static and Dynamic Electricity.* McGraw–Hill, 3rd ed., 1968.

[15] J. Sliško and R. A. Brito-Orta, "On approximate formulas for the electrostatic force between two conducting spheres," *American Journal of Physics*, Vol. 66, No. 4, 1998, pp. 352–355.

[16] S. Wang and H. Schaub, "Switched Lyapunov Function Based Coulomb Control of a Triangular 3-Vehicle Cluster," *Advances in Astronautical Sciences*, Vol. 135, American Astronautical Society, 2009, pp. 1477–1496. Paper AAS 09–391.

[17] H. Schaub, "Stabilization of Satellite Motion Relative to a Coulomb Spacecraft Formation," *AIAA Journal of Guidance, Control, and Dynamics*, Vol. 28, Nov.–Dec. 2005, pp. 1231–1239.

[18] A. Natarajan and H. Schaub, "Hybrid Control of Orbit Normal and Along-Track Two-Craft Coulomb Tethers," *Aerospace Science and Technology*, Vol. 13, June–July 2009, pp. 183–191.

[19] U. Yamamoto and H. Yamakawa, "Two-Craft Coulomb-Force Formation Dynamics and Stability Analysis with Debye Length Characteristics," *AIAA/AAS Astrodynamics Specialist Conference and Exhibit*, Honolulu, Hawaii, Aug. 18–21 2008. Paper No. AIAA 2008-7361.

[20] R. Inampudi and H. Schaub, "Two-Craft Coulomb Formation Relative Equilibria about Circular Orbits and Libration Points," *AAS/AIAA Spaceflight Mechanics Meeting*, San Diego, CA, Feb. 14–18 2010. Paper AAS 10–163.

[21] H. Schaub and I. I. Hussein, "Stability and Reconfiguration Analysis of a Circulary Spinning 2-Craft Coulomb Tether," *IEEE Transactions on Aerospace and Electronic Systems*, Vol. 46, October 2010, pp. 1675–1686, doi:10.1109/AERO.2007.352670.

[22] I. I. Hussein and H. Schaub, "Stability and Control of Relative Equilibria for the Three-Spacecraft Coulomb Tether Problem," *Acta Astronautica*, Vol. 65, No. 5–6, 2009, pp. 738–754, doi:10.1016/j.actaastro.2009.03.035.

[23] C. M. Saaj, V. J. Lappas, D. J. Richie, H. Schaub, and D. Izzo, "Hybrid Propulsion System for Spacecraft Swarm Aggregation using Coulomb Force," *Journal of British Interplanetary Society*, July 2007.